

# SWCX Emission from the Helium Focusing Cone — Preliminary Results

S. L. Snowden\*, K.D. Kuntz<sup>†</sup> and M. R. Collier\*\*

\*Code 662, NASA/Goddard Space Flight Center, Greenbelt, MD 20771

<sup>†</sup>The Henry A. Rowland Department of Physics and Astronomy, The Johns Hopkins University,  
Baltimore, MD 21218

\*\*Code 673, NASA/Goddard Space Flight Center, Greenbelt, MD 20771

**Abstract.** Preliminary results from an *XMM-Newton* campaign to study solar wind charge exchange (SWCX) emission from the heliospheric focusing cone of interstellar helium are presented. The detections of enhanced O VII and O VIII emission from the cone are at the  $2\sigma$  and  $4\sigma$  levels.

**Keywords:** X-rays – observations, Solar System

**PACS:** 95.55.Ka

## INTRODUCTION

The solar wind charge exchange (SWCX) emission in the heliosphere not associated with distinct objects (e.g., comets and planets including exospheric material in and near Earth's magnetosheath) is proportional to the flux of the solar wind and the space density of neutral material. The neutral material originates in the interstellar medium (ISM) and passes through the solar system due to the relative motion of the Sun and the ISM. The flow of the neutral material through the solar system is strongly perturbed by the Sun both by gravity and by radiation pressure. Because of the relative radiative scattering cross sections and the effect of solar gravitation the density of interstellar hydrogen near the Sun is reduced while interstellar helium is gravitationally focused. This creates a helium focusing cone downstream of the Sun [e.g., 1, and references therein].

## OBSERVATIONS AND DATA

### X-ray Data

In order to study the significance of SWCX emission from the solar system an observation campaign was designed to use the geometric variation of the helium focusing cone to search for a corresponding variation in the diffuse X-ray emission. Three pairs of *XMM-Newton* observations, matched pointings of the south ecliptic pole (SEP) and of the Hubble Deep Field – North (HDFN), were approved by the project and scheduled for late 2003 (see Table 1 for the observation details). The coupled observations of the HDFN were included as controls to monitor the SWCX emission variation not associated with the focusing cone (e.g., due to variations in the solar wind flux and composition) which could be from either Earth's magnetosheath or from the heliosphere.

**TABLE 1.** *XMM-Newton* Observation Details

ObsId	Observation Start	R.A.	Dec.	Exposure	Good Time
0162160101	2003-11-24 20:07:55	06 00 09.36	-66 34 15.7	13.44 ks	11.90 ks
0162160201	2003-11-24 09:18:35	12 37 01.02	62 12 57.1	15.25 ks	12.89 ks
0162160301	2003-12-05 20:47:15	06 00 07.63	-66 34 26.8	11.45 ks	8.57 ks
0162160401	2003-12-06 12:38:23	12 37 01.02	62 13 06.2	10.85 ks	9.62 ks
0162160501	2003-12-14 14:26:09	06 00 06.48	-66 34 34.8	11.45 ks	9.32 ks
0162160601	2003-12-14 23:15:09	12 37 01.70	62 13 16.0	43.17 ks	10.06 ks
0111550201	2001-05-18 22:17:34	12:36:50.00	62:13:12.0	41.88 ks	34.89 ks
0111550401	2001-06-01 08:16:36	12:36:57.00	62:13:30.0	91.99 ks	26.73 *ks

\* Data from the low SWCX emission part of the observation.

The orbit of *XMM-Newton* is highly elongated (perigee  $\sim 10^4$  km, apogee  $\sim 10^5$  km) and inclined (inclination  $\sim 40^\circ$ ) relative to the equatorial plane. In late November and early December, while Earth is near or over the focussing cone, the time period for these observations, the apogee lies in the anti-solar direction. This is fortuitous for two reasons: since observations take place away from perigee any SWCX emission from the magnetosheath is significantly reduced [e.g., 2] and the likelihood of soft proton contamination is also reduced [3].

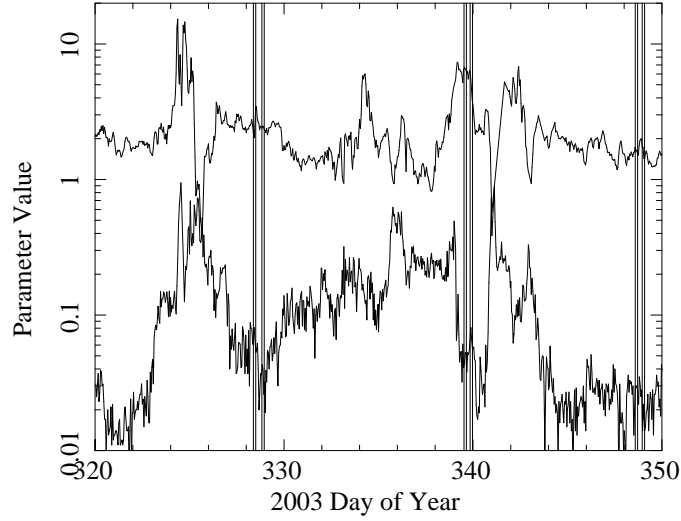
We reduced the EPIC MOS data using the *XMM-Newton* ESAS<sup>1</sup> analysis package [4] as demonstrated in Snowden et al. [5]. The data are first screened for variations in the light curve which indicate either excesses in the normal internal particle background and more commonly contamination by soft protons [3]. In either case the affected time periods are excluded from the analysis. Next, data from the full field of view were extracted after the exclusion of point sources to a limit to  $10^{14}$  ergs  $\text{cm}^{-2}$   $\text{s}^{-1}$ . Finally model particle background spectra are produced for subtraction during the spectral fitting process.

After extraction the spectra were fit using a complicated model including three thermal components (an unabsorbed 0.1 keV model for local emission and absorbed 0.1 keV and  $\sim 0.3$  keV models for a two-component halo) and an absorbed power law representing the cosmic background, monochromatic lines at 1.49 keV and 1.75 keV representing the internal fluorescent Al and Si background, and a power law not folded through the instrumental response representing any residual soft proton contamination left after the screening process. APEC thermal spectral models with variable abundances were used where the abundance of oxygen was set to zero and the other abundances were fixed at 1 (based on the assumption that oxygen will dominate any SWCX emission in the *XMM-Newton* bandpass). Monochromatic lines at 0.56 keV and 0.65 keV were added to the model to represent all observed oxygen emission, both SWCX and of more distant cosmic emission, the latter which produces a constant offset. The absorption of the halo thermal components and the power law were fixed at the Galactic values. A spectrum derived from the *ROSAT* All-Sky Survey (RASS) data was simultaneously fit with the oxygen emission coming from the thermal models rather than the monochromatic lines.

<sup>1</sup> [http://heasarc.gsfc.nasa.gov/docs/xmm/xmmhp\\_xmmesas.html](http://heasarc.gsfc.nasa.gov/docs/xmm/xmmhp_xmmesas.html)

**TABLE 2.** Fitted Line Fluxes in LU

ObsId	Target	O VII Flux	O VIII Flux	Normalized O VII Flux	Normalized O VIII Flux
0162160101	SEP	9.22±0.64	3.70±0.33	6.13±0.85	0.93±0.31
0162160201	HDFN	9.69±0.59	4.18±0.33	—	—
0162160301	SEP	9.88±0.68	3.95±0.42	7.04±1.01	1.69±0.61
0162160401	HDFN	9.04±0.67	2.45±0.34	—	—
0162160501	SEP	8.27±0.64	2.81±0.34	8.27±0.64	2.81±0.34
0162160601	HDFN	6.44±0.66	1.05±0.33	—	—
0111550201	HDFN	10.40±0.45	2.62±0.24	—	—
0111550401	HDFN	8.80±0.52	2.77±0.27	—	—



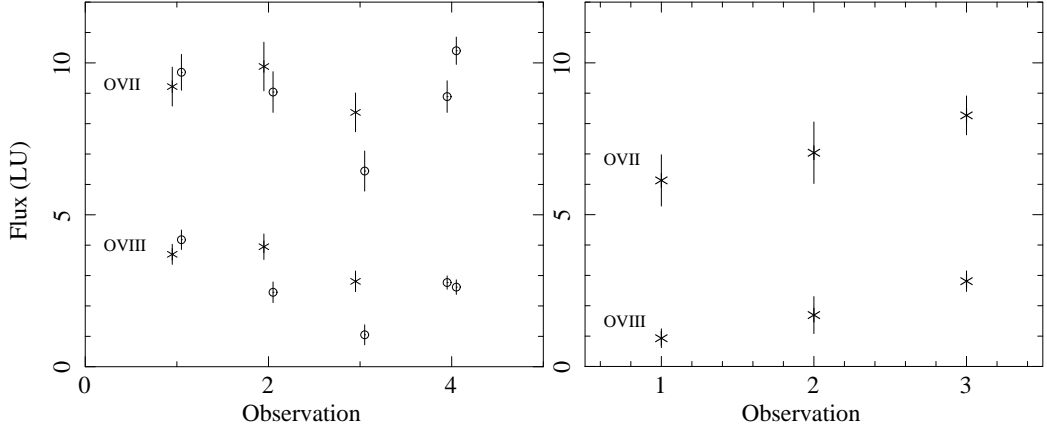
**FIGURE 1.** *ACE* solar wind proton flux (upper curve, units of  $10^8$  particles  $\text{cm}^{-2} \text{s}^{-1}$ ) and the  $\text{O}^{+7}/\text{O}^{+6}$  density ratio data (lower curve) covering the time interval of the observations. The vertical lines show the individual observation intervals.

Table 2 lists the fitted values for the O VII and O VIII flux in line units (LU, photons  $\text{cm}^{-2} \text{s}^{-1} \text{sr}^{-1}$ ). Also included are results from the spectral fits from two of the HDFN spectra from Snowden et al. [6]. The data are also plotted in Figure 2—*left*.

## Solar Wind Data

The *ACE* satellite at the L1 point provides density and velocity (among other quantities) measurements of various species in the solar wind. Since SWCX emission is proportional to the flux of the solar wind species producing the emission, the *ACE* data can be used to gain insight into the variation of the observed flux. Figure 1 shows the solar wind proton flux and the  $\text{O}^{+7}/\text{O}^{+6}$  density ratio for the period of this program (the observation intervals are shown by the vertical lines).

Both the solar wind proton flux and the oxygen density ratio show significant but



**FIGURE 2.** **Left:** Fitted values for the O VII (upper grouping of points) and O VIII line fluxes (lower grouping of points). Data points with an X symbol are in the direction of the SEP, data points with a circle symbol are in the direction of the HDFN. The pairs of points at observations 1 – 3 are (0162160101, 0162160201), (0162160301, 0162160401), and (0162160501, 0162160601), respectively. The observation 4 data points are from two HDFN spectra (0111550201, 0111550401). **Right:** The SEP line fluxes after using the HDFN data to normalize flux. See text for a listing of the caveats concerning such a normalization.

not unusual variation over the interval. It is unfortunate that the data which are the most relevant, the actual  $O^{+8}$  and  $O^{+7}$  fluxes, are not readily available from the *ACE* instruments and the two displayed parameters must act as surrogates for at least a qualitative understanding of the circumstances.

## ANALYSIS

The data as plotted in Figure 2—*left* show very considerable scatter. Any expected trend of the first SEP (off-cone) pointing being lower while the last two pointings [on-cone, the first at the nominal cone position, the second at the secondary cone position of 7] being higher is completely obscured. However, the HDFN results can be used to attempt a normalization the SEP data. As noted above, the observations took place while the *XMM-Newton* satellite was on the opposite side of Earth from the Sun. This geometry minimizes the SWCX emission from in and near the magnetosheath [2]. The observed SWCX X-ray emission in this case may then be dominated by the heliosphere, and we will make this assumption. We also note that because the distribution of the solar wind in the heliosphere (a fall-off as the distance from the Sun squared,  $\sim R^{-2}$ ), SWCX emission in the heliosphere is dominated by interactions within the nearest few AU from the Sun. Since the solar wind travels at about a quarter of an AU per day, the observed heliospheric SWCX emission represents an averaging of the solar wind parameters over a time scale of a week or two.

The HDFN observations are used as a control to monitor the variation of the average solar wind effective for each pair. The pointings are to the north and should therefore be relatively unaffected by the helium focusing cone so any variation should be due to differences in the average solar wind flux rather than variation in the effective heliospheric

densities. Our second caveat, and a great leap of faith, is that the solar wind parameters are the same in the north as they are in the south. If the assumption is valid then correcting for the variation of the effective solar wind requires a simple scaling using the HDFN data, and we have done so for the data in Table 2 and Figure 2–*right*. The results clearly show enhanced values for the observations taken through the focusing cone.

There is, however, yet another caveat. Any additional O VII or O VIII emission along the line of sight outside of the heliosphere (or even a non-temporally varying amount from the heliosphere, perhaps at the heliopause) will make the scaling inaccurate and reduce the dynamic range of the observed normalized variation.

## Results

While the caveats are significant, we have likely observed SWCX emission from the helium focusing cone in the heliosphere. Comparing the first and third pointings, the excesses observed are  $2.1 \pm 1.1$  LU for O VII and  $1.9 \pm 0.5$  LU for O VIII for  $2\sigma$  and  $4\sigma$  detections, respectively. The next step is to estimate the expected variation in the observed SWCX emission produced by model distributions of the helium focusing cone. Our results here will help constrain model for both the focusing cone and SWCX emission.

## ACKNOWLEDGMENTS

This paper was based on an observation obtained with *XMM-Newton*, an ESA science mission with instruments and contributions directly funded by ESA Member States and NASA. The *ACE* Level 2 data were obtained from the *ACE* Science Center web interface. This work was supported by a NASA *XMM-Newton* GO grants.

## REFERENCES

1. J. G. Michels, J. C. Raymond, J. L. Bertaux, E. Quémerais, R. Lallement, Y.-K. Ko, D. Spadaro, L. D. Gardner, S. Giordano, R. O’Neal, S. Fineschi, J. L. Kohl, C. Benna, A. Ciaravella, M. Romoli, and D. Judge, *ApJ* **568**, 385–395 (2002).
2. I. P. Robertson, and T. E. Cravens, *Geophys. Res. Lett.* **30**, 22–1–22–4 (2003).
3. K. D. Kuntz, and S. L. Snowden, *A&A* **478**, 575–596 (2008).
4. S. L. Snowden, and K. D. Kuntz, Cookbook for analysis procedures for *XMM-Newton* EPIC MOS observations of extended objects and the diffuse background, Tech. rep., *XMM-Newton* GOF, GSFC, NASA, Greenbelt, MD 20771 (2006), URL [http://xmm.gsfc.nasa.gov/docs/xmm/xmmhp\\\_xmmsas.html](http://xmm.gsfc.nasa.gov/docs/xmm/xmmhp\_xmmsas.html).
5. S. L. Snowden, R. F. Mushotzky, K. D. Kuntz, and D. S. Davis, *A&A* **478**, 615–658 (2008).
6. S. L. Snowden, M. R. Collier, and K. D. Kuntz, *ApJ* **610**, 1182–1190 (2004).
7. M. R. Collier, T. E. Moore, D. Simpson, A. Roberts, A. Szabo, S. Fuselier, P. Wurz, M. A. Lee, and B. T. Tsurutani, *Advances in Space Research* **34**, 166–171 (2004), arXiv:astro-ph/0304368.